Experimental observations of water-like behavior of initially fluidized, dam break granular flows and their relevance for the propagation of ash-rich pyroclastic flows

Olivier Roche, Santiago Montserrat, Yarko Niño, Aldo Tamburrino

Experimental observations of water-like behavior of initially fluidized, dam break granular flows and their relevance for the propagation of ash-rich pyroclastic flows

O. Roche,[1] S. Montserrat,[2] Y. Niño,[2] and A. Tamburrino[2]

[1] The physics of ash-rich pyroclastic flows were investigated through laboratory dam break experiments using both granular material and water. Flows of glass beads of 60–90 μm in diameter generated from the release of initially fluidized, slightly expanded (2.5–4.5%) columns behave as their inertial water counterparts for most of their emplacement. For a range of initial column height to length ratios of 0.5–3, both types of flows propagate in three stages, controlled by the time scale of column free fall $\sim(h_0/g)^{1/2}$, where h_0 denotes column height and g denotes gravitational acceleration. Flows first accelerate as the column collapses. Transition to a second, constant velocity phase occurs at a time $t/(h_0/g)^{1/2} \sim 1.5$. The flow velocity is then $U \sim \sqrt{2}(gh_0)^{1/2}$, larger than that for dry (initially nonfluidized) granular flows. Transition to a last, third phase occurs at $t/(h_0/g)^{1/2} \sim 4$. Granular flow behavior then departs from that of water flows as the former steadily decelerates and the front position varies as $t^{1/3}$, as in dry flows. Motion ceases at $t/(h_0/g)^{1/2} \sim 6.5$ with normalized runout $x/h_0 \sim 5.5–6$. The equivalent behavior of water and highly concentrated granular flows up to the end of the second phase indicates a similar overall bulk resistance, although mechanisms of energy dissipation in both cases would be different. Interstitial air-particle viscous interactions can be dominant and generate pore fluid pressure sufficient to confer a fluid-inertial behavior to the dense granular flows before they enter a granular-frictional regime at late stages. Efficient gas-particle interactions in dense, ash-rich pyroclastic flows may promote a water-like behavior during most of their propagation.

1. Introduction

[2] Geophysical granular flows commonly occur in various environments, and prediction of their behavior is crucial for hazard assessment. Pyroclastic density currents represent major threats for populations and infrastructure [*Druitt*, 1998; *Freundt and Bursik*, 1998; *Branney and Kokelaar*, 2002]. They are commonly generated during volcanic eruptions by the collapse of lava domes [*Cole et al.*, 2002] or explosive eruption columns [*Sparks and Wilson*, 1976], as well as by sedimentation of dilute ash clouds when these interact with topography [*Druitt et al.*, 2002] (Figure 1). These density currents consist of hot mixtures of particles and volcanic gas and can propagate from their vent over distances of several kilometers on very gentle slopes. Analyses of the characteristics of their deposits led to the identification of two end-member conceptual models, possibly delimiting a continuum, as the parent currents are thought to be dilute, turbulent pyroclastic surges [e.g., *Fisher*, 1966; *Branney and Kokelaar*, 1992] or dense granular flows [e.g., *Sparks*, 1976; *Wilson*, 1986]. Our study focuses on dense flows, being in most cases a rapidly moving basal dense granular avalanche overridden by a dilute ash cloud [*Denlinger*, 1987; *Fisher*, 1995].

[3] Prediction of the behavior of pyroclastic flows can be achieved through analytical and numerical simulations provided that the physics and derived constitutive relationship for flow motion are known, and this represents a challenging issue. Insights into the general flow behavior are obtained from analytical calculations [*Denlinger*, 1987; *Beget and Limke*, 1988; *Levine and Kieffer*, 1991], and an accurate mode of emplacement can be investigated from numerical simulations. As for other types of geophysical flows, the aim of the numerical simulations is to solve the equations of conservation of mass and momentum introducing a closure for the resistance of the flow. Pyroclastic flows have been the focus of several studies based on more or less sophisticated methods, including kinetic [*McEwen and Malin*, 1989; *Saucedo et al.*, 2005; *Wadge et al.*, 1998],

[1]Laboratoire Magmas et Volcans, OPGC, Université Blaise Pascal, IRD, CNRS, Clermont-Ferrand, France.
[2]Department of Civil Engineering, Universidad de Chile, Santiago, Chile.

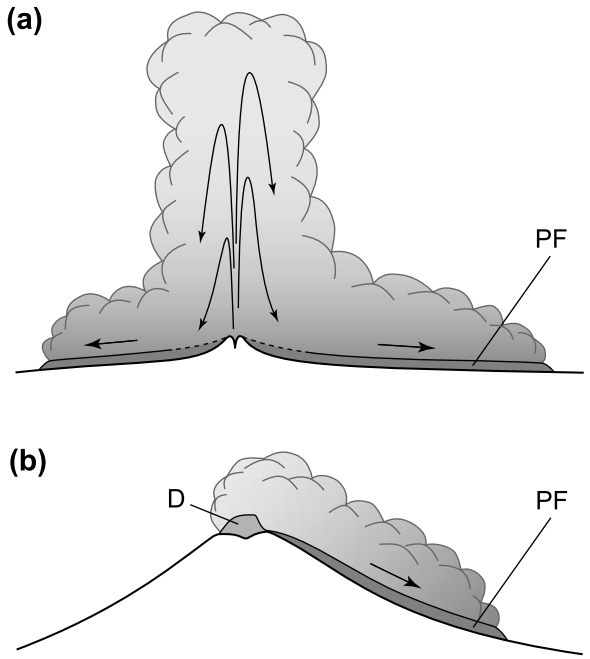

Figure 1. Schematic representation of pyroclastic flow generation mechanisms. Gravitational collapse of (a) a large eruptive column and (b) a lava dome. PF and D denote pyroclastic flow and dome, respectively.

depth average [*Sheridan et al.*, 2005; *Kelfoun et al.*, 2008; *Mangeney et al.*, 2007], and multiphase [*Valentine and Wohletz*, 1989; *Neri et al.*, 2007] approaches. One of the major limitations of these models is the nature of the resistance stress, which is assumed to be frictional Coulomb-type or constant, viscous (proportional to the flow velocity, U), inertial-turbulent (proportional to U^2), or a combination of these (see for instance the related analysis for two-phase flows by *Ancey* [2007]).

[4] Information on the processes governing pyroclastic flows can be obtained from extensive works on the physics of granular flows. However, despite intensive research, the fundamental mechanisms of these flows are still controversial and the nature of the constitutive equations represents a matter of debate, particularly when interstitial fluid effects can become important [*GDR MiDi*, 2004; *Forterre and Pouliquen*, 2008]. Dense flows with particle concentrations close to maximum packing of the static material have been the focus of several studies, as summarized for instance by *GDR MiDi* [2004]. Inertia is recognized as important within those flows, but more important are interparticle collisional and frictional contacts that resist motion and dissipate energy. Seminal experimental and theoretical works commonly considered the steady regime on inclines at angles close to the angle of repose ($\sim 30^\circ$) of the granular material. The analysis assumes a frictional rate-independent Coulomb-type friction law [*Savage*, 1984; *Savage and Hutter*, 1989] or that energy dissipation results from both frictional and collisional contacts [*Johnson and Jackson*, 1987; *Johnson et al.*, 1990]. Later works revealed a complex form of energy dissipation, as friction is depth-dependent [*Pouliquen*, 1999] and flow rheology is of viscoplastic nature characterized by a yield shear stress and a complex dependence on shear rate [*Jop et al.*, 2006; *Forterre and Pouliquen*, 2008].

[5] In pyroclastic flows, fluidization of the granular mass by an upward flow of gases of internal sources or air ingested is assumed to be a major mechanism that controls the dynamics of emplacement and adds complexity to their understanding [*Sparks*, 1978; *Wilson*, 1980, 1984; *Druitt et al.*, 2007]. For instance, experimental studies on continuously fluidized flows on an inclined or horizontal substrate, for which basal and internal friction are considerably reduced, revealed that the internal velocity profiles and segregation processes can be different from those of non-fluidized cases [*Ishida et al.*, 1980; *Takahashi and Tsujimoto*, 2000; *Eames and Gilbertson*, 2000]. The aim of the present experimental study was to investigate unsteady granular flows generated from the quasi-instantaneous release of a static gas-fluidized column. No subsequent source of gas is provided during flow emplacement. The purpose of initial fluidization of the granular column is to weaken the contact forces in the particles' chain network in order to investigate how this imposed initial condition influences the subsequent flow dynamics. This extends earlier works by *Roche et al.* [2002, 2004, 2005], which revealed that initially fluidized granular flows share some similarity with buoyancy-driven gravity currents of pure Newtonian fluid. Similar experiments were also carried out recently by *Girolami et al.* [2008] with pyroclastic material. The reader may refer to work by *Fan and Zhu* [1998] and *Rhodes* [1998] for the fundamentals of gas fluidization and to work by *Wilson* [1980, 1984] and *Druitt et al.* [2007] for aspects more specific to pyroclastic materials.

[6] In the present study, we carried out dam break-type experiments with granular material and investigated a range of different initial column aspect ratios in a rectangular reservoir, as considered in experiments with flows in which the interstitial fluid has no effect [*Balmforth and Kerswell*, 2005; *Lajeunesse et al.*, 2005; *Lube et al.*, 2005]. In order to determine to what extent the behavior of a dense granular flow, initially fluidized or not, is comparable to that of a pure fluid under dam break conditions, we also carried out experiments using water in the same flume. For this, we studied the flow kinematics quantitatively using appropriate time and length scales. Our results reveal that the interstitial air within dense granular flows can have a fundamental influence as these behave like their water counterparts for most of their emplacement. This is what we mean by water-like behavior throughout this paper.

2. Principles of Dam Breaking

[7] We investigated unsteady flows of dense granular matter on the basis of the dam break concept, which is a classical issue in the context of engineering applications dealing with catastrophic flows of water or mixtures of water and particles [*Chow*, 1959; *Graf and Altinakar*, 2000]. The seminal analysis by *Ritter* [1892] considers a 2-D open channel flow, propagating on a horizontal surface, generated from the quasi-instantaneous release of a material initially at rest in a reservoir of height h_0, which is considered as semi-infinite (Figure 2). Ritter's depth-averaged analysis neglects frictional and turbulent resistive effects and assumes hydrostatic pressure conditions and negligible vertical acceleration. The flow depth is predicted to decrease monotonically as the consequence of the formation of two waves, one

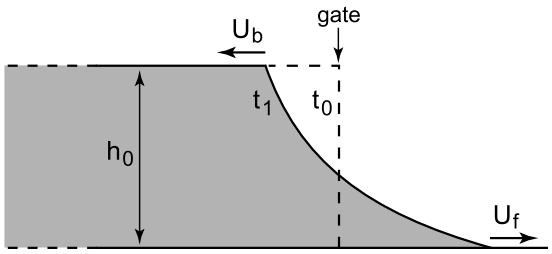

Figure 2. The concept of dam breaking [*Ritter*, 1892]. The case of an ideal frictionless fluid propagating on a dry substrate is shown before (t_0) and after (t_1) the opening of the sluice gate. Two waves propagate, one forward in the channel at speed $U_f = 2(gh_0)^{1/2}$ and the second backward in the reservoir at $U_b = (gh_0)^{1/2}$.

retreating backward in the reservoir at a speed $U = (gh_0)^{1/2}$ and the second propagating into the channel at a higher speed $U = 2(gh_0)^{1/2}$. Since this earlier work, the dam break issue has received much attention, and subsequent studies developed more sophisticated analyses and particularly addressed flow resistance by introducing a hydraulic resistance term [*Dressler*, 1954; *Whitham*, 1955]. Following these classical approaches, experiments on dam break flows of water commonly dealt with reservoirs having a height much smaller than their length [*Dressler*, 1954; *Bell et al.*, 1992; *Lauber and Hager*, 1998; *Jánosi et al.*, 2004; *Leal et al.*, 2006]. *Leal et al.* [2006], in particular, reviewed several experimental studies that reveal that water flows propagate into the channel at a speed of $U \sim \sqrt{2}(gh_0)^{1/2}$, lower than that predicted by *Ritter* [1892]. Recently, *Hogg and Woods* [2001] and *Hogg and Pritchard* [2004] presented theoretical analyses of the dam break problem, specifically addressing flow resistance in these unsteady flows and providing reasonable interpretation of experimental observations. This is further discussed in section 5.1 in connection with our experimental results.

3. Experimental Device and Procedure

[8] Dam break experiments with granular matter or water were conducted in an experimental apparatus consisting of a reservoir and a horizontal channel separated by a vertical sluice gate (Figure 3). The apparatus is made of smooth Perspex plates. For experiments on granular flows, the reservoir is equipped with a basal porous plate through which air is introduced vertically from a wind box to generate a fluidized granular column [*Roche et al.*, 2002]. Air is dried by means of filters, and its flux is controlled by a series of manometers. The channel is 3 m long, and both the reservoir and the channel have widths of 10 cm. Transparent lateral walls allow for video analysis of the emptying reservoir and propagation of the flow in the channel. The initial column height in the reservoir (h_0) and reservoir length (x_0) were varied so that h_0 is in the range from 10 to 40 cm and x_0 is in the range from 10 to 20 cm, and we considered aspect ratios

$$r = \frac{h_0}{x_0} \tag{1}$$

of 0.5–3.

[9] For granular flows, we used glass beads of grain size d in the range from 60 to 90 μm (d_{50} = 75 μm) and density ρ_s = 2500 kg m^{-3}, with a loose packing volume fraction c_0 = 0.58 ± 0.02 so that the bulk density of a granular column is ρ_b = 1450 ± 50 kg m^{-3}. Before each experimental run, the particles were subjected to an intense flux of dry air in a fluidization rig in order to reduce as much as possible the cohesion effects caused by ambient moisture. Then, particles were poured into the reservoir, and the granular column could be fluidized by means of a flux of dry air passing through the basal porous plate. As air ascends into the granular pile, the drag force generated counterbalances the weight of the grains, thus, reducing substantially the intensity of the interparticle contacts in the force chain network. The particles used belong to group A of *Geldart*'s [1973] classification that describes the behavior of gas-particle fluidization. This means that particulate (homogeneous) fluidization is possible over a range of gas flow velocity, which is observed for many industrial materials but also for samples of ash-rich pyroclastic flow deposits [*Druitt et al.*, 2007]. The granular column was fluidized at the following velocities, defined as the mean flow rate divided by the cross-sectional area of the reservoir: (1) the minimum fluidization velocity (U_{mf} = 7.5 mm s^{-1}) at which the bed is fully supported and pore fluid pressure is maximum, as the weight of the particles is balanced by the drag force caused by air motion, but the packing volume fraction is not modified, and (2) at a larger velocity (U_{mb} = 1.6–1.7U_{mf}) just before gas bubbles form and at which the maximum expansion of the column in the present case is only e = 2.5–4.5% [*Rhodes*, 1998]. It is important to note that no air flux is provided in the channel during flow propagation, so that the dynamics of emplacement is partially affected by the diffusion of the pore fluid pressure generated in the initially fluidized granular column. For comparison, flows were also generated from granular

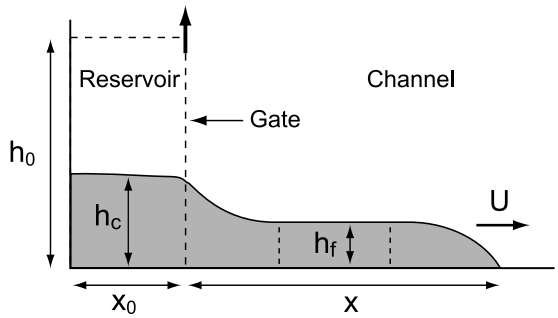

Figure 3. Sketch of the experimental device used for dam break experiments with both granular matter and water. Material is released from the reservoir into the channel by means of a vertical sluice gate (vertical dashed arrow). For granular flows, the initial column can be fluidized by means of an air flux introduced at the base of the reservoir through a porous plate. Initial conditions are the initial column height in the reservoir (h_0) and reservoir length (x_0). Kinematic parameters are the collapsing column height in the reservoir (h_c), the mean height of the flow in the channel estimated as the average height of the central third (h_f), the flow front position from the gate (x), and the flow front velocity (U).

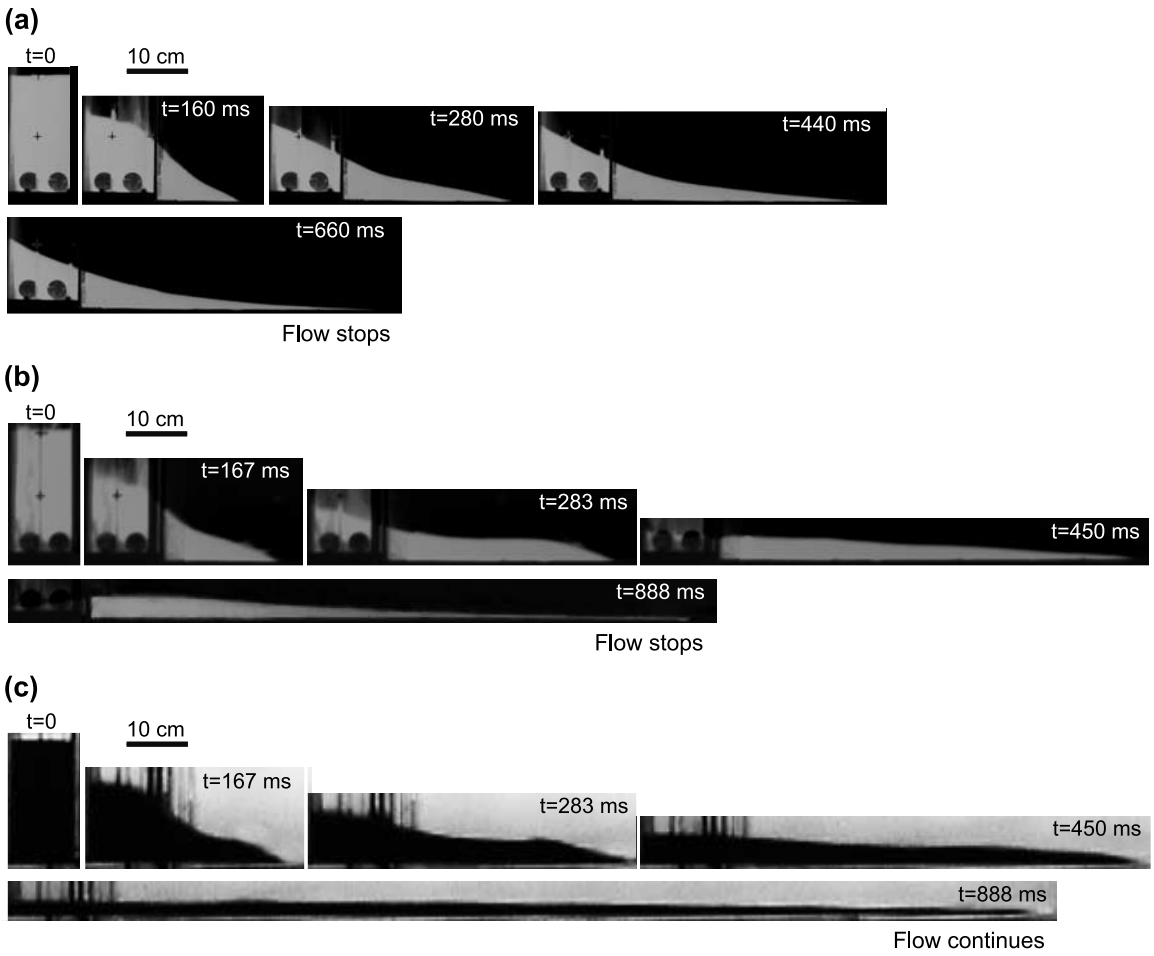

Figure 4. Snapshots of dam break flows (time in milliseconds). Flows generated from columns (h_0 = 20 cm, x_0 = 10 cm, and r = 2) of (a) dry granular material; (b) fluidized, slightly expanded (e = 2.5–4.5%) granular material with air velocity U_{mb} in the reservoir; and (c) water (dyed). After release, Figures 4b and 4c propagate at almost constant height and velocity (e.g., t = 283 ms), and water flows are inertial at that stage. Initially fluidized granular flow behavior departs from that of water flows only when the column height has decreased to almost the flow height at the entrance of the channel (t > 450 ms).

columns with no air flux in the reservoir, and these are called dry hereafter. For experiments with water, we used a reservoir with an impermeable base. Great care was taken to ensure that no filtration occurred at the sluice gate and that the channel was perfectly dry before release of the static liquid column. Flows of water always reached the open end of the channel and were collected in a tank. Water spread until surface tension forces dominate, thus leaving a thin liquid layer of about 2 mm. In order to facilitate video analysis, water in the reservoir was dyed with natural pigments, and the rear part of both the reservoir and the channel was covered with tracing paper in order to provide uniform illumination when lighted from behind. Experiments were recorded at 30–90 frames s^{-1}, and a mark adapted to the sluice gate allowed for accurate determination of the moment at which opening began. Videos were analyzed to determine kinematic parameters describing flow motion, such as the column height in the reservoir (h_c), the mean height of the flow in the channel (h_f), and the flow front position from the gate (x) (Figure 3). The mean flow height was estimated as the average height of the central third of the current for convenience. This provides a good estimate of the mean height of the entire flow as it is thicker near the gate and thins at the front in the same proportion. We did not detect significant wall effects on the flow height, and it was rather constant in the cross section.

4. Experimental Results

4.1. Characteristics of Flow Kinematics

[10] Under the range of initial configurations, all types of granular flows formed a deposit whose longitudinal extent was lower than the channel length. Flow duration and runout were 0.66–1.28 s and 0.60–2.20 m, respectively, for initial granular columns fluidized at U_{mb}; 0.56–1.04 s and 0.43–1.55 m for columns fluidized at U_{mf}; and 0.46–0.92 s and 0.23–1.01 m for dry columns. Flows of water and granular material resulting from fluidized columns have a very similar morphology for most of their emplacement (Figure 4). The drag exerted by the sluice gate when it is suddenly removed affects only a very thin layer of the column and has a negligible influence on the bulk flow behavior. Once the gate is open, flows are generated from

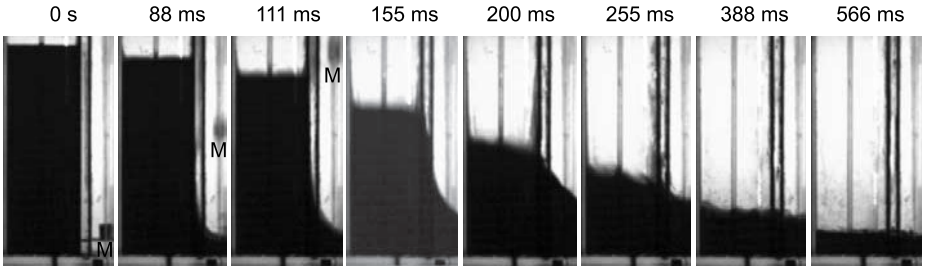

Figure 5. Vertical descent of the water column within the reservoir (h_0 = 30 cm, x_0 = 10 cm, and r = 3). M indicates the mark on the sluice gate, and numbers indicate time.

the bottom of the column and material is evacuated from the reservoir. A surface dam break wave propagates backward in the reservoir at $r \leq 1.5$, as predicted by *Ritter*'s [1892] analysis. In contrast, the column drops vertically with little deformation of the top at $r > 1.5$ (Figure 5). Then, flows propagate at an almost constant height for a while. This contrasts with dry flows that are generated from flank avalanches and propagate as wedges, as described previously [*Roche et al.*, 2002, 2004; *Balmforth and Kerswell*, 2005; *Lajeunesse et al.*, 2005; *Lube et al.*, 2005]. Finally, flows spread into the channel, and granular flows finally come to halt, whereas water flows continue past the channel end. Deposits of the granular flows resulting from fluidized columns have a horizontal upper surface in the reservoir, where the material thickness is slightly less than that at the entrance of the channel. Within the channel, their upper surface dips gently toward the front at an angle of about $1-2^\circ$. This contrasts with deposits resulting from dry granular columns as the slope angle of their upper surface in the reservoir is close to the angle of repose of the material ($\sim 30^\circ$) and the thickness steadily decreases downstream.

[11] Flows emplace in three distinct stages, and dry flows depart significantly from the others (Figure 6). During the first, collapse phase, flows generated from granular columns fluidized at U_{mf} or U_{mb} and from water columns steadily accelerate at low h_0 ($\leq$20 cm) or enter almost immediately into a first constant velocity phase at high h_0 (>20 cm). The flow height in the channel steadily increases while the column height decreases as the reservoir empties at a nearly constant rate. Dry flows propagate at slower velocities, and at a given time their height in the channel is significantly higher than that of the other types of flows. Then, water and initially fluidized granular flows enter into a second, constant velocity phase. Transition between the first and second phases occurs when the flow height in the channel has a maximum value ($h_f \sim 0.2h_0$), whereas the column height is

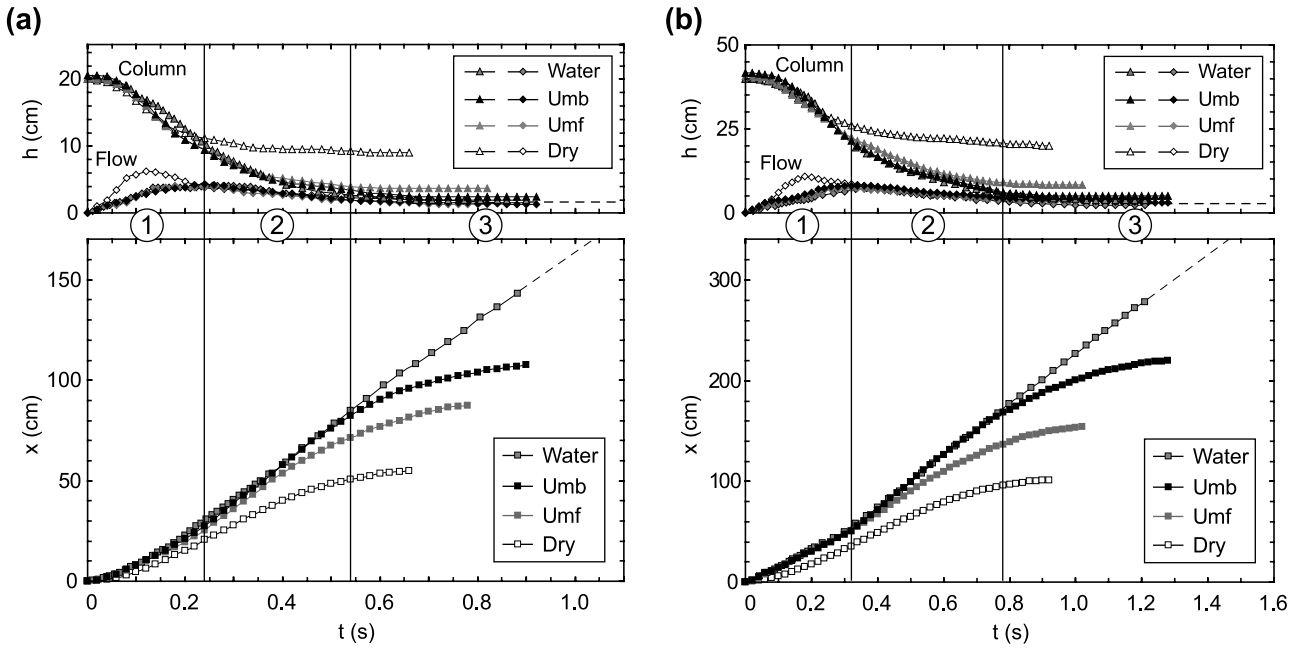

Figure 6. Kinematic data of dam break flows. Flow kinematics for reservoir aspect ratio r = 2, with flow front position (x), and column and flow height (h) as a function of time (t) for (a) h_0 = 20 cm and x_0 = 10 cm and (b) h_0 = 40 cm and x_0 = 20 cm. Numbers in circles correspond to phases 1 (column collapse), 2 (constant velocity), and 3 (stopping phase of granular flows). Granular flows generated from columns fluidized at U_{mb} behave as water flows until transition between phases 2 and 3. Dashed lines indicate that water flows continue. Dry flow behavior clearly departs from that of other types.

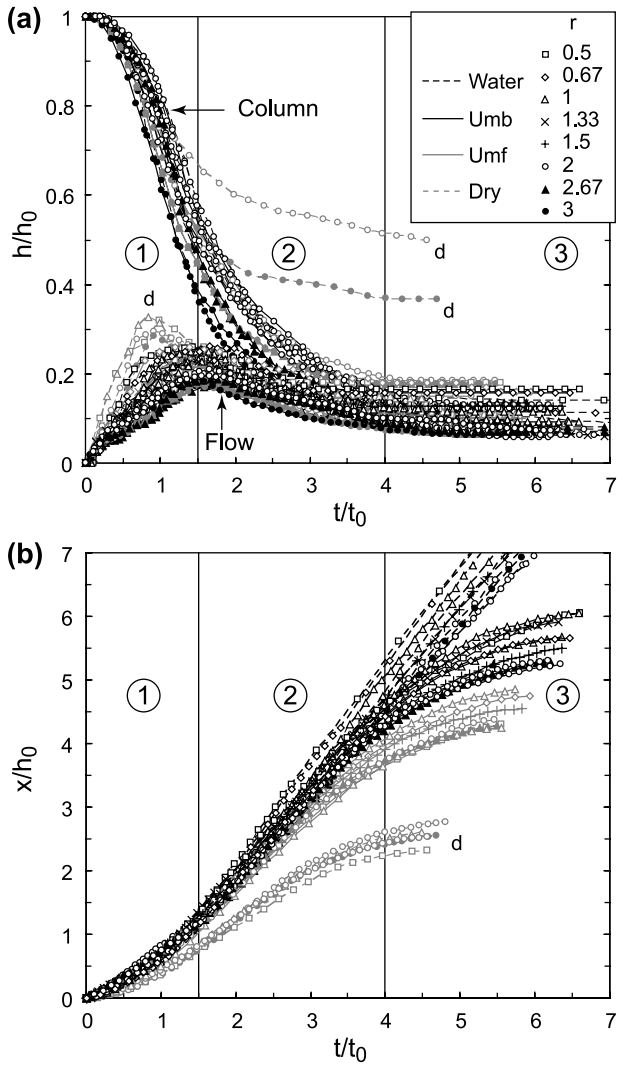

Figure 7. Nondimensional kinematic data of dam break flows. Data are shown for various reservoir aspect ratios r with normalized (a) column and flow height h/h_0 and (b) flow distance x/h_0 as a function of time t/t_0, with $t_0 = (h_0/g)^{1/2}$. Data for the column height are shown when the column collapses with little deformation of the top ($r > 1.5$). Numbers in circles correspond to phases 1 (column collapse), 2 (constant velocity), and 3 (stopping phase of granular flows). Dry granular flows are marked with a d in the plot.

about half its initial value. In the case of high initial reservoir height, this transition corresponds to a sudden acceleration of the front (Figure 6b). During most of the second phase, the flow height in the channel is approximately constant, except at the entrance of the channel and at the flow front (Figure 4). A notable result is that granular flows resulting from initially fluidized, slightly expanded columns (at U_{mb}) and water flows propagate at almost the same velocity. Water flows are inertial at that stage, as the Reynolds number

$$Re = \frac{\rho_w U h_f}{\mu_w} \tag{2}$$

is 3×10^4–2×10^5, where ρ_w and μ_w are the density and dynamic viscosity of water, respectively, and U is the flow front velocity. Granular flows generated from nonexpanded fluidized columns (at U_{mf}) propagate less rapidly, whereas the column height in the reservoir and the flow height in the channel are similar to those of flows of water and those resulting from slightly expanded fluidized columns (at U_{mb}). Compared to other cases, dry flows are significantly slower during this stage although their height in the channel has acquired about the same value, and the column height in the reservoir is now much larger. Transition to a last, third phase is identified from the data of water flows and that of granular flows generated from columns fluidized at U_{mb}. This occurs when the column height has dropped to almost that of the flow in the channel, i.e., when the driving pressure between the material in the reservoir and the channel has reduced significantly. The behavior of the initially fluidized (at U_{mb}) granular flows only departs from that of water flows at that stage. Although data of flow and column heights are similar, those of the flow front position clearly deviate from each other. During this third phase, water flows propagate at a velocity slightly smaller than that in the second phase, whereas the granular flows steadily decelerate. It is worth noting that our first (acceleration) and second (constant velocity) phases correspond to the slumping phase described for fluid gravity currents [*Huppert*, 2006].

4.2. Collapse of the Kinematic Data

[12] The behavior of the dam break flows investigated in our study can be characterized quantitatively through scaling considerations. For this, we determined appropriate time and length scales in order to collapse the kinematic data of the experiments over a range of initial column aspect ratios in the reservoir (r = 0.5–3). We considered length scales x_0, h_0, or $(x_0 h_0)^{1/2}$ and time scales $(x_0/g)^{1/2}$, $(h_0/g)^{1/2}$, or $x_0/(gh_0)^{1/2}$ and tested all possible combinations to plot normalized data of length as a function of time. We conclude that the appropriate time scale is $(h_0/g)^{1/2}$, which is proportional to the characteristic time of free fall of the column, $(2h_0/g)^{1/2}$, whereas the relevant length scale is h_0, the initial column height in the reservoir. Other time and length scales do not lead to collapse of the data for the range of reservoir aspect ratios considered. The characteristic time and length scales we used were proposed already to describe the motion of dam break flows of water with reservoirs having a very low aspect ratio ($r \ll 1$) [*Leal et al.*, 2006], and our experiments offer the opportunity to test the relevance of those characteristic scales for reservoirs with a higher aspect ratio. We note that the length scale chosen by earlier works to describe the motion of dry granular flows is the reservoir length x_0 [*Lube et al.*, 2004; *Lajeunesse et al.*, 2005], and this issue is addressed hereafter.

[13] Figure 7 shows collapse of the data for water and initially fluidized granular flows over the range of reservoir aspect ratios investigated, and emplacement in three distinct phases is controlled by the time scale $(h_0/g)^{1/2}$. Transition between the first (collapse) and the second (constant velocity) phases occurs at dimensionless time $t/(h_0/g)^{1/2} \sim 1.5$, with $h_c/h_0 \sim 0.5$ and maximum flow height $h_f/h_0 \sim 0.2$. At that stage, data collapse of the flow front position for each flow type is very good, whereas the normalized flow or column

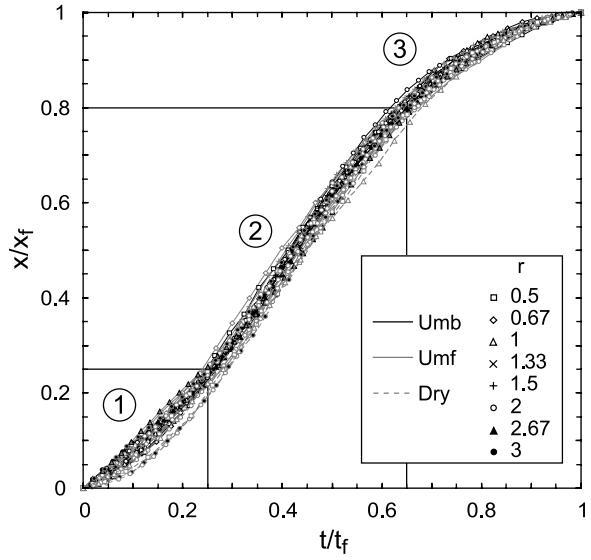

Figure 8. Kinematic data of the granular flows normalized with the runout distance (x_f) and the flow duration (t_f) for the whole range of reservoir aspect ratios investigated (r = 0.5–3). All flows have the same relative duration and distance of propagation for the three phases of emplacement.

height slightly decreases when the reservoir aspect ratio increases. It is worth noting that gate opening is rapid as its base is above the top of the collapsing column at times $t/(h_0/g)^{1/2}$ less than about 0.3–0.5 (see also Figure 5). Transition to the last, third (stopping) phase as the column height in the reservoir has dropped to almost that of the flow in the channel occurs at $t/(h_0/g)^{1/2} \sim 4$. During this phase, normalized flow and column height both tend to 0.07–0.15. There is a tendency for the normalized flow front position to slightly decrease as the reservoir aspect ratio increases. However, initially fluidized granular flows have similar relative durations, t_f, so that $t_f/(h_0/g)^{1/2} \sim 5.5$–6 and $t_f/(h_0/g)^{1/2} \sim 6$–6.5 at initial airflow velocity in the reservoir U_{mf} and U_{mb}, respectively. On the other hand, motion ceases at normalized distance $x/h_0 \sim 4.5$–5 (at U_{mf}) and $x/h_0 \sim 5.5$–6 (at U_{mb}). Compared to dry cases, initial fluidization of the granular column in the reservoir enhances the relative flow duration and runout by a factor of ~1.2–1.4 and ~1.8–2.2, respectively. Dry granular flows depart from others, as they propagate at lower front velocity with transition between the first and the second phases occurring earlier and with greater maximum flow height. The data of the column height in the reservoir do not collapse under this normalization. However, the data of the flow front position do collapse, both in space and time.

[14] The relative duration and distance of propagation of the three phases of emplacement are the same for the three types of granular flows investigated. Figure 8 reveals very good collapse of the front position, x, data as a function of time, when using the runout, x_f, and t_f as length and time scales, except maybe for dry flows during the first phase. The transition between the first and second phases occurs at ~25% of the flow duration and runout, whereas that between the second and third phases occurs at ~65% of the flow duration and ~80% of the runout. During the third, stopping phase, granular flows generated from fluidized columns behave as their dry counterparts. When kinematic data (x versus t) are plotted in logarithmic scales, the best fit of the values when flows decelerate and before their motion ceases (third phase) gives slopes of 0.30–0.35, and we assume that the normalized flow front position varies with time to the power 1/3 (Figure 9).

[15] Analysis of the kinematic data of our dam break experiments shows that the characteristic time and length scales, $(h_0/g)^{1/2}$ and h_0, respectively, used previously to describe the kinematics of dam break flows of water generated from reservoirs having very low aspect ratios [*Leal et al.*, 2006], are also relevant in the case of reservoirs of high aspect ratios (at least up to 3), for which no backward wave in the reservoir occurs, and the column rather collapses vertically as gravitational acceleration is preponderant. We emphasize that the length scale x_0 used in previous studies on dry granular flows [*Lube et al.*, 2004; *Lajeunesse et al.*, 2005] is less appropriate for collapsing the kinematic data over the range of initial column aspect ratios tested (r = 0.5–3). Figure 10 shows the flow front position normalized using x_0 instead of h_0 (x/x_0). In that case, collapse of the data is possible only for the same values of the initial aspect ratio, and this applies to all types of flows considered in this study, i.e., water flows and initially fluidized and dry granular flows. We note that collapse of the data for all aspect ratios is readily obtained if x/x_0 is renormalized as $(x/x_0)/r = x/h_0$, as shown in Figures 7 and 9.

4.3. Flow Dynamics

[16] The dynamics of the flows can be investigated through analysis of the Froude number (i.e., the normalized flow velocity) during the first phase and/or the second phase

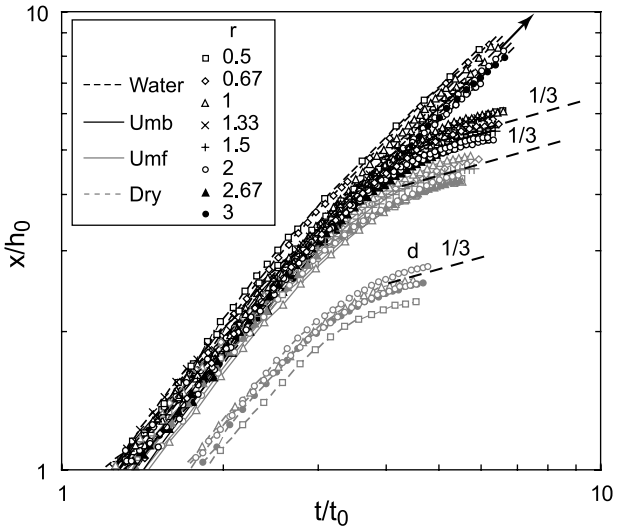

Figure 9. Stopping phase of the granular flows. Flow kinematics shown for various reservoir aspect ratios r with normalized flow distance x/h_0 and time t/t_0, with $t_0 = (h_0/g)^{1/2}$ in a log-log plot. The arrow indicates that water flows continue. Granular flows, including dry ones (noted d), steadily decelerate during the third, stopping phase as the front position varies as $t^{1/3}$ before they come to a halt (dashed lines).

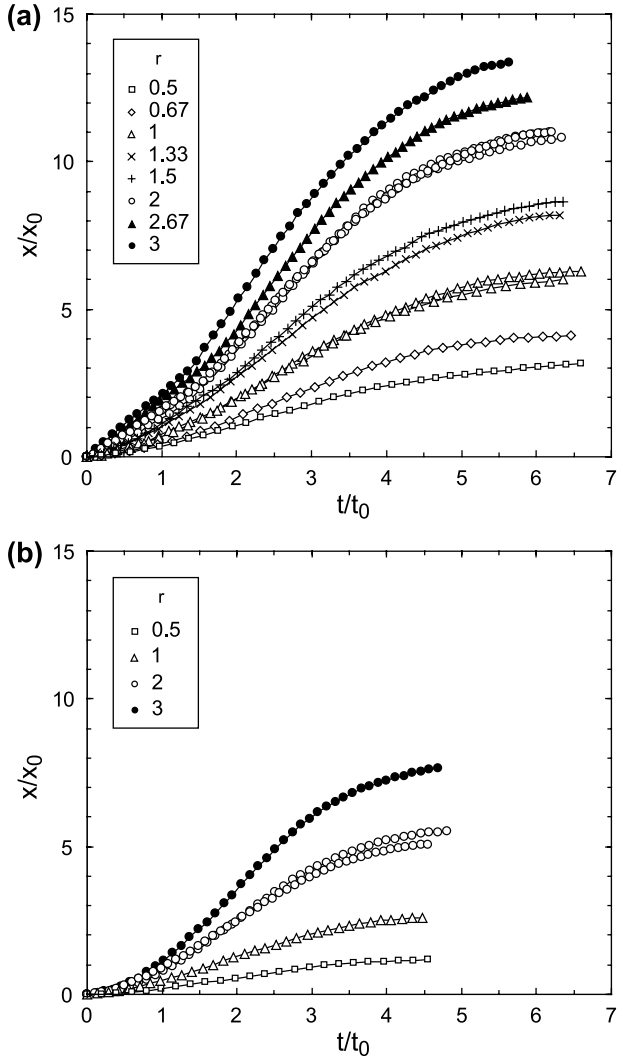

Figure 10. Kinematic data of the granular flows generated from columns (a) fluidized at U_{mb} or (b) with no air flux (dry), shown for various reservoir aspect ratios r, with normalized flow distance x/x_0 and time t/t_0, with $t_0 = (h_0/g)^{1/2}$. The data collapse only for experiments at the same r (i.e., 1 and 2).

as the front velocity is nearly constant. We calculated the source Froude number, defined as

$$Fr_0 = \frac{U}{(gh_0)^{1/2}}, \tag{3}$$

and we note that this is also the slope in Figure 7b. Values of Fr_0 in the first phase can be determined for flows of water and those generated from fluidized granular columns and propagating at almost constant velocity at that stage, i.e., for cases at sufficiently high initial reservoir height ($h_0 >$ 20 cm). The calculation can be made in all cases for the second phase. The results in Figure 11 reveal that, for the first phase, values of Fr_0 decrease from about 1.2 to 0.7 as the reservoir aspect ratio increases from 1 to 3 but are independent of the type of flow. In the second phase, the source Froude number is independent of the reservoir aspect ratio. In flows of water and those generated from slightly expanded granular columns fluidized at U_{mb}, Fr_0 has a similar value, as a matter of fact, close to the theoretical value $\sqrt{2}$ for a steady orifice flow [*White*, 2003], and this issue is addressed in section 5.1. In nonexpanded granular flows initially fluidized at U_{mf}, values of Fr_0 are lower, in the range from about 1 to $\sqrt{2}$. Dry granular flows have even lower values as $Fr_0 \sim 0.9$–0.95.

[17] Further insights into the flow dynamics are obtained through analysis of the flow Froude number, defined as

$$Fr = \frac{U}{(gh_f)^{1/2}}. \tag{4}$$

The results are shown in Figure 12 as a function of the normalized time, and we note that $Fr = Fr_0/(h_f/h_0)^{1/2}$. Once again, the data for dry flows are clearly distinguishable from the others. During the first phase, of approximately constant front velocity (at $h_0 >$ 20 cm), the flow Froude number decreases with time as the flow height in the channel increases. Values for the initially fluidized granular flows tend to be slightly lower than those of water flows. We observe a sudden acceleration between the first and second phases, thus, explaining a sharp transition at $t/(h_0/g)^{1/2} \sim$ 1.5 in Figure 12, as mentioned in section 4.2 for data in Figure 7. Thus, Fr increases as flows enter the second phase and propagate at a larger (also approximately constant) front velocity. For flows of water and of granular matter initially fluidized at U_{mb}, Fr is approximately constant and in the range 2.8–3.2 during a time interval $t/(h_0/g)^{1/2} \sim 0.5$. Then, it increases gradually to about 3.5–4 as the flow height decreases. Granular flows generated from columns fluidized at U_{mf} propagate in the second phase at lower Fr values of about 2.5–3.

5. Discussion

5.1. Mechanisms of Dam Breaking

[18] The results of our experiments on dam break flows are now compared to those of similar works carried out with water or dry granular material. Our experiments on flows resulting from the release of water or fluidized granular columns reveal notable differences from *Ritter*'s [1892] simple model. At reservoir aspect ratios larger than about 1.5, no wave propagates backward in the reservoir, and the column rather collapses vertically with its upper surface remaining almost flat and horizontal (Figure 5). This shows that gravitational acceleration cannot be neglected to describe dam break flows generated from reservoirs of high aspect ratios. The flow in the channel propagates at a front velocity $U \sim \sqrt{2}(gh_0)^{1/2}$, independent of the initial reservoir aspect ratio for r = 0.5–3. This velocity is lower than the value predicted for the ideal frictionless case for which $U = 2(gh_0)^{1/2}$ [*Ritter*, 1892]. This means that resistance introduces important retardation of flow motion. We emphasize that the flow front velocity we determined in our study is consistent with observations made in water dam break experiments, as reviewed by *Leal et al.* [2006, Figure 3]. Their water flows are generated from reservoirs having low aspect ratios ($r \ll 1$), and their front velocity is given by $U \sim \sqrt{2}(gh_0)^{1/2}$ over normalized time $t/(h_0/g)^{1/2}$ and distances x/h_0 of about 5 and 6, respectively and subsequently

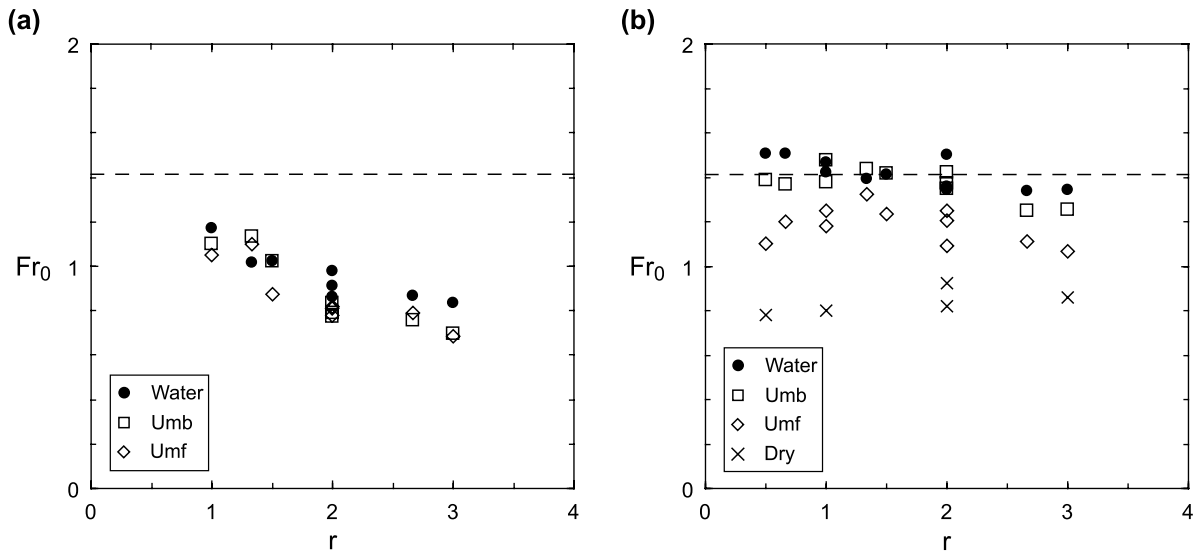

Figure 11. Source Froude numbers of the flows $Fr_0 = U/(gh_0)^{1/2}$, as a function of the reservoir aspect ratio r, for (a) the first and (b) the second phases of emplacement. The dashed line indicates that the theoretical value $Fr_0 = \sqrt{2}$ for a steady orifice flow. In Figure 11a, data correspond to experiments with water and initially fluidized granular flows and of initial column height $h_0 > 20$ cm, i.e., to flows that propagate at constant velocity.

decreases slowly. Interestingly, our data show that this flow front velocity is the same for a large range of reservoir aspect ratios.

[19] In recent theoretical analyses of dam break flows of a pure fluid, *Hogg and Woods* [2001] and *Hogg and Pritchard* [2004] showed that in the inertial regime, with negligible internal viscous forces, motion results from a balance between the streamwise gradient of hydrostatic pressure (buoyancy), fluid inertia, and resistance (presumably dominated by drag at boundaries). *Hogg and Pritchard* [2004] tested various resistance terms in their depth average models, assuming that resistance at boundaries derives from (1) viscous effects ($\xi \sim \mu(U/h)^{\alpha}$), where ξ is the resistance stress, μ is dynamic viscosity, h is the flow depth, and α is some exponent; (2) Coulomb-like friction (ξ proportional to ρgh) that is uniform throughout the fluid domain, where ρ is the fluid density; or (3) shear drag associated with turbulent fluid motion (ξ proportional to ρU^2). They compared their results to those of some experimental studies and concluded that models with a turbulent, Chezy-type drag term having the form $\xi = \rho C_d U^2$, where C_d is a drag coefficient with a value of 0.001–0.01, best describe the motion of dam break flows of a pure Newtonian fluid. They showed that drag, which is applied on the whole extent of the flow, has a

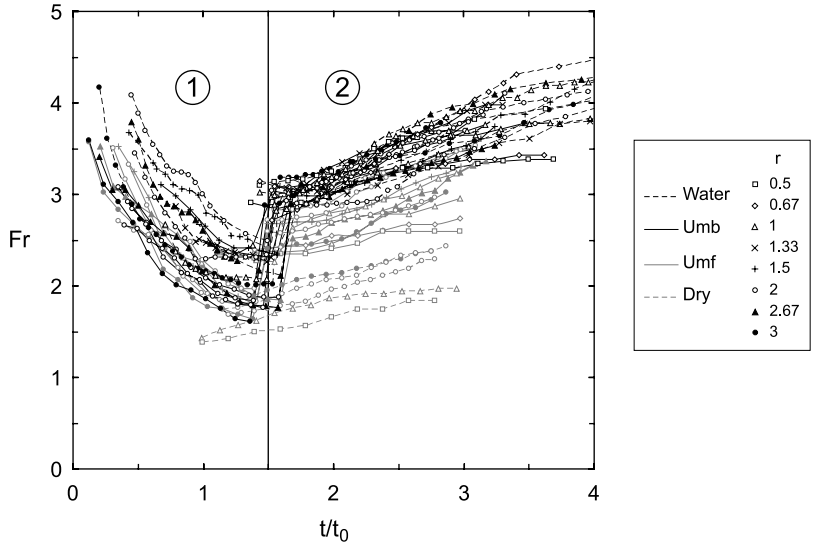

Figure 12. Flow Froude number $Fr = U/(gh_f)^{1/2}$ as a function of normalized time t/t_0, with $t_0 = (h_0/g)^{1/2}$, for the first and second phases of emplacement of all types of flows. A sharp transition occurs at $t/t_0 \sim 1.5$ as a sudden acceleration between the two phases is observed.

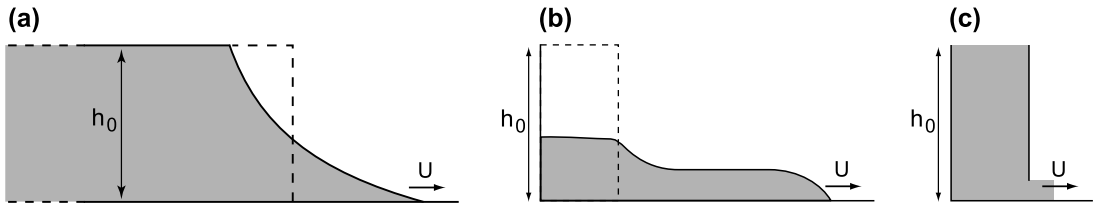

Figure 13. Schematic representation of flows propagating at front velocity U (a) in the case of ideal frictionless dam breaking, $U = 2(gh_0)^{1/2}$ [*Ritter*, 1892]; (b) in this study, $U \sim \sqrt{2}(gh_0)^{1/2}$; and (c) for a steady orifice flow, $U = \sqrt{2}(gh_0)^{1/2}$.

greater effect at the flow front where the local driving pressure is small because of small height, and in consequence the fluid builds up and the front steepens to increase the pressure gradient, which counters the flow resistance. The distance over which drag at boundaries has a significant influence is expected to increase with time. The calculated front velocity is smaller than that predicted if drag at boundaries is neglected, so that $U/(gh_0)^{1/2} = Fr_0 = 2$ [i.e., *Ritter*, 1892], and $U/(gh_0)^{1/2} = Fr_0$ is slightly less than about $\sqrt{2}$ [*Hogg and Pritchard*, 2004, Figures 9 and 11]. This latter value depends on the drag coefficient. We note that the value of $\sim\sqrt{2}$ is also the one we determine in our experiments, which suggests that the processes that generate resistance acting in the laboratory flows we tested could be comparable to those described by *Hogg and Pritchard* [2004] and that the drag coefficient in our experiments (with water and initially fluidized granular flows) would be similar.

[20] Flows generated in dam break conditions result basically from the collapse of the initial column under the influence of gravity once the sluice gate is removed. In consequence, it is interesting to find that the source Froude number (Fr_0) has a value close to that corresponding to a steady frictionless orifice flow, which is somewhat paradoxical as the material is progressively evacuated from the reservoir in our experiments and the flows are dissipating energy as they propagate along the channel (Figure 13). Nonetheless, as already discussed, this can be theoretically explained by the *Hogg and Pritchard* [2004] analysis.

5.2. Water-Like Behavior of Initially Fluidized, Dense Granular Flows

[21] Our experiments show that, under dam break conditions, granular flows generated from slightly expanded columns (fluidized at U_{mb}) have the same kinematics as inertial water flows, as long as motion is driven by a pressure gradient between the reservoir and the channel. According to our description, this occurs during the first (collapse) and the second (constant velocity) phases, until normalized time $t/(h_0/g)^{1/2} \sim 4$ and distance $x/h_0 \sim 4.5$. This suggests that, at those stages, the overall balance between inertia, hydrostatic pressure gradient (buoyancy) and resistance, typical of inertial fluid gravitational flows [*Hogg and Pritchard*, 2004] is, in these dense granular flows, similar to that of flows observed in water dam break experiments. Furthermore, on the basis of the *Hogg and Pritchard* [2004] analysis, the fact that the value of the source Froude number observed in the initially fluidized (at U_{mb}) granular flows is about the same as that of water flows (observed in our and previous experiments, so that $Fr_0 \sim \sqrt{2}$) suggests that the drag coefficient in both types of flows would be (1) of the inertial turbulent form and (2) possibly of the same value. This represents the main result of our study and provides new insights into the physics of dense granular flows.

[22] The overall energy dissipation derives from interactions between the flow and its boundaries and also from internal processes in the case of the granular flows. *Iverson* [1997] showed that for fluid-particle flows internal energy dissipation can result from particle contact interactions such as friction and collisions, viscous shear and turbulent velocity variation of the interstitial fluid, and drag (of viscous or inertial origin) between the particles and the interstitial fluid. He proposed a series of dimensionless numbers aimed to assess the relative magnitude of the different stresses, and we refer to some of them hereafter. In our dry granular flows, particle interactions are a dominant source of energy dissipation, as shown by their slow velocity of propagation and small runout (Figures 6 and 7). Under dam break conditions, these flows have been modeled following different approaches including discrete element and shallow water methods [*Kerswell*, 2005; *Zenit*, 2005; *Larrieu et al.*, 2006; *Doyle et al.*, 2007], and at least qualitative agreement with experimental data [*Balmforth and Kerswell*, 2005; *Lajeunesse et al.*, 2005; *Lube et al.*, 2005] has been achieved. Our results suggest that friction and collisions are very much reduced in initially fluidized granular flows, although these emplace at almost maximum concentration, and this serves as a base for the following discussion. These flows propagate at the same velocity as that of water flows when the initial column expansion is only 2.5–4.5%, and it is interesting to note that this velocity is only slightly smaller when the initial column is not expanded, if fluidized at U_{mf}. This suggests that once contact forces in the chain network of the initial granular column are dramatically weakened, reversal to a frictional and collisional regime during flow emplacement is very much delayed.

[23] Buffering of particle interactions resulting from slow diffusion of the initial pore pressure caused by air flux in the reservoir is very unlikely, as discussed by *Roche et al.* [2004]. The pore pressure diffusion time scale is $t_d \sim h_f^2/D$ [*Iverson*, 1997], where D is the pore pressure diffusivity of the granular material. *Montserrat et al.* [2007] have shown that $D \sim 0.02$ m^2 s^{-1} for the granular material used in the experiments reported here. This means that if we consider a typical mean flow height in the channel of 0.02–0.08 m, then the initial excess pressure is eliminated in only 3–6% of the flow duration once the flow enters the channel.

[24] On the other hand, flow dynamics is not governed by the interstitial air dynamic viscosity (μ_a) in our experiments, as shown by corresponding values of the Bagnold number [*Bagnold*, 1954; *Iverson*, 1997]:

$$Ba = c^* \frac{\rho_s \gamma d^2}{\mu_a}, \tag{5}$$

where $c^* = [c^{1/3}/(c_0^{1/3} - c^{1/3})]^{1/2}$, with c denoting concentration of the material during flow propagation; c_0 is the maximum concentration at loose packing; and γ is the shear rate, which is typically considered to be equal to U/h_f for the computation and analysis of Ba and other relevant dimensionless parameters [e.g., *Iverson*, 1997]. The Bagnold number represents a measure of the ratio of particle collisional stresses to fluid viscous shear stresses. For the range of experiments investigated, $Ba \sim 280-970$, which is above the upper limit value of $\sim$45 for a macroviscous regime [*Bagnold*, 1954]. Alternatively, the highest Ba values ($>\sim$450) could suggest significant interparticle collisions. This interpretation, however, has been challenged by *Hunt et al.* [2002], who showed that if a collisional regime probably exists at lower particle concentrations and higher shear rates, the limit proposed by *Bagnold* [1954] is not valid and derives from a misinterpretation of his experimental results. *Iverson* [1997] proposed an alternative Bagnold number, Ba', with $c^* = c/(1 - c)$, such that a fluid-particle flow is then dominated by collisional contacts at $Ba' > \sim$200. In our experiments $Ba' \sim 150$, below the limit value proposed by *Iverson* [1997], suggesting that energy dissipation through interparticle collisions, if present, would not be a dominant process. Furthermore, large values of Ba' may not necessarily imply the occurrence of a collisional regime, as the interstitial fluid dynamics coupled to unsteady particle motion can damp particle contact interactions under certain conditions [*Iverson*, 1997; *Iverson and LaHusen*, 1989], as discussed hereafter.

[25] Significant fluctuating energy has been observed in fluidized beds of particles of group A [*Cody et al.*, 1996; *Biggs et al.*, 2008], such as those of our experiments, indicating that unsteady particle motion can be relevant in our flows at least during the initial stages of emplacement. Because of this, our dense granular flows could be dominated by interactions between the particles and the interstitial air, as shown for continuously fluidized slow flows or vibrated beds [*Eames and Gilbertson*, 2000; *Burtally et al.*, 2002]. Air-particle interactions, along with drag at boundaries, could confer to these highly concentrated granular media a behavior similar to that of inertial water flows. The intensity of these interactions can be estimated using the Darcy number [*Iverson*, 1997], which represents the ratio of viscous fluid-particle interaction stresses to particle inertial stresses, so that

$$Da = \frac{\mu_a}{kc\rho_s\gamma}, \tag{6}$$

where k is the permeability of the granular medium ($\sim 10^{-12}$ m^2 in this study). In this definition Darcy's law for viscous stresses in the interstitial fluid is assumed to be valid. It is well known that for flow in a porous medium Darcy's law is valid for particle Reynolds number, defined as

$$Re_p = \frac{v\delta\rho_a}{\mu_a}, \tag{7}$$

where v is the bulk velocity of the interstitial fluid flow; δ is a characteristic size of the interstices; and ρ_a is the air density, lower than about 1–10 [*Rhodes*, 1998]. In the case of a granular flow, we are interested in describing the motion of the fluid relative to the particles. Following *Iverson* [1997], we can estimate that $v\delta \sim \gamma d^2$, where d is the particle diameter representative of the granular medium. Using this result and replacing (7) in (6), we obtain

$$Da = \frac{\rho_a}{\rho_s}\frac{d^2}{Re_p kc}. \tag{8}$$

Imposing the limit $Re_p < 1-10$, we conclude that in our experiments for Darcy's law to be valid, Da needs to be larger than about 2–20. Estimating Da in our experiments, we obtain values in the range $\sim$170–370. This implies two things, first that the fluid-particle interactions in our flows are purely viscous (no inertial coupling; that is, Darcy's law is valid) and second, that viscous fluid-particle interaction stresses are dominant over particle inertial stresses because of the large values of Da obtained. A similar conclusion is reached if one considers the ratio of viscous fluid-particle interaction stresses to particle (frictional) shear stresses, which, on the basis of *Iverson's* [1997] analysis, would be proportional to $\gamma\mu_a d/[c(\rho_s - \rho_a)gk]$. In our experiments, this ratio is 2–3 orders of magnitude smaller than the maximum value required for Darcy's law to be valid (i.e., $Re_p < 1-10$), thus, showing that viscous fluid-particle interactions stresses are also dominant over particle shear stresses.

[26] *Iverson* [1997] suggested, probably on the basis of the experimental study reported by *Iverson and LaHusen* [1989], that the Darcy number also describes the tendency for pore fluid pressure developing between moving grains to buffer particle interactions. According to *Iverson and LaHusen* [1989] unsteady motion of grains can produce pore pressure that is able to locally support normal and shear stresses, while grain contacts transiently vanish. The pore pressure generated can then propagate to adjacent areas, which, in turn, can generate shear zone growth. As viscous fluid-particle interaction stresses are dominant over both particle inertial and shear stresses in the present initially fluidized granular flows (i.e., high values of Da), we may infer that pore pressure is likely to be generated in the moving granular mass, which would promote buffering of grain interactions. Additionally, air may act as a thin cushion between the particles and damp interparticle contacts as the grains are agitated during flow emplacement. The fluctuating energy (i.e., granular temperature) initially imposed to the particles when they are fluidized in the reservoir could additionally participate in

the enhanced mobility of the flows. As a matter of fact, significant granular temperature was observed in fluidized beds of particles of group A [*Cody et al.*, 1996] and it is maximum for conditions close to U_{mb} [*Biggs et al.*, 2008], which coincide with those that create the granular flows with the longest runout in our experiments.

[27] We note that in initially slightly expanded granular flows (fluidized at U_{mb}), a return to a compacted state is likely to be achieved during the (first) collapse phase. Assuming that the sedimentation time scale is $t_s \sim eh_f/U_s$, where $U_s \sim 8$ mm s^{-1} is the fall velocity of the top of the static granular bed in the reservoir determined from collapse tests, this represents only 5–12% of the flow duration. This contrasts with experiments of *Girolami et al.* [2008] carried out with initially highly expanded material (e up to ~50%), which revealed that the flow runout is controlled by the sedimentation time scale of the flowing mixture. However, this conclusion was not valid for initial expansion less than 7%, as is the case in our experiments. Besides, as already discussed, the time scale of initial pore pressure diffusion is also small compared with the flow duration (3–6%). Thus, air-particle differential motion and associated pore pressure generation during flow emplacement are expected to derive mainly from continuous rearrangement of the granular network, as shown for water-particle flows [*Iverson and LaHusen*, 1989]. Indeed, self-fluidization has been observed in recent experiments by *Bareschino et al.* [2008] on granular flows in a rotating tank using group A particles. These experiments show that a fluid-like behavior can be obtained at sufficiently high shear rates. The authors argue that air, which in their experiments is assumed to be entrained at the flow front through small-scale avalanches, is the key factor to conferring the fluid-like behavior to these flows.

[28] When the pressure gradient between the material in the reservoir and in the channel has decreased ($h_c \sim h_f$), the flow velocity is not sufficient to confer a fluid-inertial (water-like) behavior to the granular material. In consequence, air-particle interactions are less efficient and the behavior of the initially fluidized granular flows returns rapidly to that of their dry counterparts, which are dominated by interparticle friction. The associated Savage number, which represents the ratio of particle collisional stresses to frictional stresses, defined as

$$Sa = \frac{\rho_s \gamma^2 d^2}{(\rho_s - \rho_a) g h_f}, \tag{9}$$

is about 10^{-6}, much less than the upper limit value of 0.1 for the frictional regime [*Savage and Hutter*, 1989]. During the third, stopping phase of emplacement, the flow front position of both types of flows then varies as $t^{1/3}$ until motion ceases (Figure 9).

[29] Recent research has suggested a viscoplastic constitutive law for describing the rheology of dry, dense frictional granular flows [*Forterre and Pouliquen*, 2008]. This law is basically of Coulomb-type, where the local shear stress is proportional to the normal stress. The proportionality factor, or friction coefficient, would not be a constant but would depend on a dimensionless parameter, the inertial number, which is a ratio of a microscopic time scale representing the time scale for a particle to fall in the interstices of the granular medium and a macroscopic time scale related to the mean shear rate. The inertial number is equivalent to the square root of the Savage number defined above. In the case where the interstitial fluid becomes important for the behavior of the flow, *Courrech du Pont et al.* [2003] and, later, *Cassar et al.* [2005] have proposed a modified version of the inertial number to account for the effects of the interstitial fluid as particles move into the granular network. *Naef et al.* [2006] have also supported the use of viscoplastic constitutive laws for granular flows, such as Bingham. However, in the inertial regime, typical of high-velocity flows such as debris flows or snow avalanches, other relationships combining turbulence closures and Coulomb-type friction lead to better results when simulations are compared to natural data [see also *Bartelt et al.*, 1999]. Our results support the concept of a constitutive law that is strongly dependent on the shear rate. Furthermore, the present observations suggest the existence of a combined effect of fluid-particle interactions, which confer on the flow an inertial behavior, and shear rate-dependent Coulomb friction as described by *Forterre and Pouliquen* [2008]. Even though the dependence of the Coulomb friction on shear rate has been proposed in the model described by *Forterre and Pouliquen* [2008], we note that in our flows the effect is of a different nature. Indeed, we observed that as the shear rate decreases, the transition from an inertial to a frictional regime occurs, such that Coulomb friction becomes dominant only at late stages of flow emplacement. Before that, the inertial component is dominant, and this leads to a resistance law that is similar to that typical for turbulent fluid flows. Interestingly, *Naef et al.* [2006] pointed out that although an inertial-type of resistance can lead to adequate simulations of debris flow motion, it is insufficient to describe cessation of motion, for which a yield stress or Coulomb friction must be taken into account.

5.3. Insights Into the Physics of Pyroclastic Flows

[30] Our dam break experiments reveal that a slight expansion of an initial granular column is sufficient to confer on the resulting flow a behavior similar to that of an inertial fluid flow for most of its emplacement because strong viscous fluid-particle interactions can develop. In this context, a continuous source of gas is not required to maintain the mixture in a fluidized state. In nature, granular expansion at least equal to that in experiments is readily achieved in case of sedimentation from an eruptive column or a dilute ash cloud and can also be obtained when a dense basal avalanche is agitated while propagating down a rough substratum (e.g., Figure 1). In experiments, the condition required for a water-like behavior is a pressure gradient derived from a difference in height, even very small, between the reservoir and the channel material. In nature, the driving pressure may derive from the height difference between the top of a large eruptive column and the resulting flow in case of propagation on rather flat areas (Figure 1a; and our experiments may be considered as simple analogs of this) or from the gradient of the free surface of the flow as

this propagates down a steep slope, in the case of small columns or collapsing domes (Figure 1b).

[31] Our results support the pyroclastic flow modeling approach by *Levine and Kieffer* [1991], based on open channel hydraulic theory. In their model, the flow is assumed to be confined, fully turbulent (inertial), and incompressible with uniform density. The simulation of *Levine and Kieffer* [1991] successfully reproduced the observed velocity ($\sim$5–30 m s^{-1}) of the pyroclastic flows produced at Mount St. Helens on 7 August 1980, which propagated on slopes of $\sim$15° in the upper parts and of $\sim$2° in distal areas. This approach is appealing in the context of hazard assessment as it requires only topographic data, a volumetric flow rate, and a Manning resistance coefficient. Accurate topographic data can be obtained for most volcanoes, and volumetric flow rates can be estimated considering a given eruption style (i.e., column or dome collapse). Even though our results suggest that the drag coefficient in our initially fluidized granular flows would be similar to that of our laboratory water flows, we would not recommend the use of typical values of the Manning or other friction coefficients for water flows in rivers to simulate the motion of pyroclastic flows. The issue of determining appropriate resistance coefficients for pyroclastic flows deserves further research.

[32] Our experiments are applicable to natural cases provided that dynamic similarity applies. In this context, we stress that the results we obtain in our experiments with initially slightly expanded granular flows that emplace as water flows are possible because we used group A particles [*Geldart*, 1973]. These particles allow for homogeneous dense phase expansion, though very small, which provides conditions for efficient viscous fluid-particle interactions to develop throughout the granular network. Previous similar experiments with coarser group B and D particles have shown that initially fluidized granular flows return to a frictional granular regime immediately after release [*Roche et al.*, 2002, 2004]. Laboratory investigations have shown that, in fact, ash-rich pyroclastic material behaves as group A particles when gas fluidized [*Druitt et al.*, 2007], and this suggests that the type of fluid-particle interactions inferred to act in our experimental flows could likely occur in highly concentrated, ash-rich pyroclastic flows. Furthermore, the inertial behavior of the laboratory flows suggests that the basic scaling determined in this paper could also apply to field-scale pyroclastic flows, which would most likely also be inertial. The viscous fluid-particle interaction effect we have pointed out in this study may buffer the interparticle friction and collisions. We have argued that viscous fluid-particle interactions are controlled by the Darcy number, which in our experiments reaches sufficiently high values so that these interactions are dominant. For pyroclastic flows, calculation of the Darcy number is not straightforward as one needs to assess the permeability, shear rate, and mean grain size because of the particle Reynolds number requirement (i.e., $Re_p < 1-10$). However, considering likely estimations for ash-rich pyroclastic flows, the values of the Darcy number in these flows can still be above the critical value for viscous fluid-particle interactions to be dominant. With these assumptions, dense, ash-rich pyroclastic flows can then be expected to propagate on simple topographies (with a continuously decreasing slope) as inertial fluid flows during most of their emplacement and would enter a granular-frictional regime at late stages. However, any positive brake in slope could accelerate the flow, which would return to a fluid-inertial regime.

6. Conclusion

[33] The present work on dam break flows of both granular matter and water on a horizontal surface brings new insights into the physics of granular flows and has important implications for the emplacement mechanisms of dense, ash-rich pyroclastic flows. Experiments were carried out for a wide range of aspect ratios of the reservoir (r = 0.5–3). They show that dense granular flows can propagate similarly to their inertial water counterparts provided that they are generated from a fluidized, slightly expanded column (e = 2.5–4.5%) and as long as motion is driven by a sufficiently high-pressure gradient between the reservoir and the channel. Analysis of the kinematic data reveals that the relevant length scale is the initial reservoir height (h_0) and that flow emplacement occurs in three phases controlled by the time scale of free fall of the column proportional to $(h_0/g)^{1/2}$. The flows experience a first (collapse) phase, and a transition to a second (constant velocity) phase occurs at normalized time $t/(h_0/g)^{1/2} \sim 1.5$ and distance $x/h_0 \sim 1.2$, representing about one fourth of the flow duration and runout. During that second phase, initially fluidized, slightly expanded granular flows and water flows propagate at a nearly constant front velocity $U \sim \sqrt{2}(gh_0)^{1/2}$, about 1.5 times faster than dry granular flows. Transition to a last, third phase occurs at $t/(h_0/g)^{1/2} \sim 4$ and $x/h_0 \sim 4.5$, representing about 65 and 80% of the flow duration and runout, respectively, when the height of the column in the reservoir has decreased to about that of the flow in the channel. During this last phase of emplacement, flows of water decelerate slightly, whereas those of granular matter enter into their stopping phase as they steadily decelerate before motion ceases at $t/(h_0/g)^{1/2} \sim 6.5$ and $x/h_0 \sim 5.5$–6. The flow front position of the initially fluidized granular flows varies as $t^{1/3}$, as observed also for dry granular flows.

[34] These observations suggest that the interstitial gas can damp dramatically particle-particle interactions in granular flows. Viscous, air-particle interactions can be the dominant process in these flows, thus, conferring to the two-phase mixture a behavior similar to that of water or any other inertial fluid flow. Once contact forces of the force chain network are strongly decreased or possibly eliminated, then return to frictional-collisional behavior typical of dry granular flows is very much delayed as motion is driven by gravity. A slight expansion of the granular medium is sufficient to confer on the resulting flow a fluid-inertial behavior, thus, contrasting fundamentally with that of dry granular flows. Flows of initially fluidized, slightly expanded granular matter may be characterized by the same resistance law as that of flows of water for most of their emplacement, corresponding to the first (collapse) and second (constant velocity) phases in the dam break conditions. As particle interactions are very much reduced, one can envisage that they are (1) totally negligible or (2) weak

and act along with viscous air-particle interactions as internal sources of energy dissipation. Our results suggest that gas-dominated granular flows can be modeled using the hydraulic theory for flows of inertial fluids, as long as motion occurs at a sufficiently high shear rate, whose threshold is to be characterized in more detail. Transition to a second behavior, typical of dry granular flows dominated by particle interactions, must then be taken into account to describe flow motion accurately.

[35] This experimental study has implications for the emplacement of dense, ash-rich pyroclastic flows, as it brings new insights into their physics and helps to identify the most appropriate approaches for their modeling. The flow behavior will be twofold: (1) inertial fluid-like at sufficiently high shear rate (this is likely to represent most of the flow emplacement) and (2) then frictional-granular at late stages. In this context, analyses combining resistance terms of inertial-turbulent (ξ proportional to ρU^2) and Coulomb frictional (ξ proportional to $\rho g h$) form appear to be appropriate tools for simulating the emplacement of these pyroclastic flows.

[36] **Acknowledgments.** This work was supported by the Institut de Recherche pour le Développement (IRD, France), ACI-INSU (France), ANR (France), and ECOS-Conicyt C06U01 (France-Chile) projects and Université Blaise Pascal. S.M. thanks the financial support from MECESUP under project UCH0310 in the form of a Ph.D. fellowship and Departamento de Postgrado y Postítulo de la Vicerrectoría de Asuntos Académicos, Universidad de Chile, in the form of a foreign residence fellowship. An earlier draft benefited from stimulating discussions with Tim Druitt and Jeremy Phillips. Sarah Fagents and two anonymous reviewers are thanked for fruitful reviews.

References

Ancey, C. (2007), Plasticity and geophysical flows: A review, *J. Non Newtonian Fluid Mech.*, *142*, 4–35, doi:10.1016/j.jnnfm.2006.05.005.

Bagnold, R. A. (1954), Experiments on a gravity-free dispersion of large solid spheres in a Newtonian fluid under shear, *Proc. R. Soc. London, Ser. A*, *225*, 49–63.

Balmforth, N. J., and R. R. Kerswell (2005), Granular collapse in two dimensions, *J. Fluid Mech.*, *538*, 399–428, doi:10.1017/S0022112005005537.

Bareschino, P., A. Marzocchella, P. Salatino, L. Lirer, and P. Petrosino (2008), Self-fluidization of subaerial rapid granular flows, *Powder Technol.*, *182*, 323–333, doi:10.1016/j.powtec.2007.12.010.

Bartelt, P., B. Salm, and U. Gruber (1999), Calculating dense snow avalanche runout using a Voellmy-fluid model with active/passive longitudinal straining, *J. Glaciol.*, *45*, 242–254.

Beget, J. E., and A. J. Limke (1988), Two-dimensional kinematic and rheological modeling of the 1912 pyroclastic flow, Katmai, Alaska, *Bull. Volcanol.*, *50*, 148–160, doi:10.1007/BF01079679.

Bell, S. W., R. C. Elliott, and M. H. Chaudhry (1992), Experimental results of two-dimensional dam-break flows, *J. Hydraul. Res.*, *30*, 225–252.

Biggs, M. J., D. Glass, L. Xie, V. Zivkovic, A. Buts, and M. A. C. Kounders (2008), Granular temperature in a gas fluidized bed, *Granular Matter*, *10*, 63–73, doi:10.1007/s10035-007-0077-8.

Branney, M. J., and P. Kokelaar (1992), A reappraisal of ignimbrite emplacement: Progressive aggradation and changes from particulate to nonparticulate flow during emplacement of high-grade ignimbrite, *Bull. Volcanol.*, *54*, 504–520, doi:10.1007/BF00301396.

Branney, M. J., and P. Kokelaar (2002), *Pyroclastic Density Currents and the Sedimentation of Ignimbrites*, 152 pp., Geol. Soc. of London, London.

Burtally, N., P. J. King, and M. R. Swift (2002), Spontaneous air-driven separation in vertically vibrated fine granular mixtures, *Science*, *295*, 1877–1879, doi:10.1126/science.1066850.

Cassar, C., M. Nicolas, and O. Pouliquen (2005), Submarine granular flows down inclined planes, *Phys. Fluids*, *17*, 103301, doi:10.1063/1.2069864.

Chow, V. T. (1959), *Open-Channel Hydraulics*, 680 pp., McGraw-Hill, New York.

Cody, G. D., D. J. Goldfarb, G. V. J. Storch, and A. N. Norris (1996), Particle granular temperature in gas fluidized beds, *Powder Technol.*, *87*, 211–232, doi:10.1016/0032-5910(96)03087-2.

Cole, P. D., E. S. Calder, R. S. J. Sparks, A. B. Clarke, T. H. Druitt, S. R. Young, R. A. Herd, C. L. Harford, and G. E. Norton (2002), Deposits from dome-collapse and fountain-collapse pyroclastic flows at Soufrière Hills Volcano, Montserrat, in *The Eruption of Soufrière Hills Volcano, Montserrat, From 1995 to 1999*, *Mem. Geol. Soc. London*, vol. 21, edited by T. H. Druitt and B. P. Kokelaar, pp. 231–262, Geol. Soc. of London, London.

Courrech du Pont, S., P. Gondret, B. Perrin, and M. Rabaud (2003), Granular avalanches in fluids, *Phys. Rev. Lett.*, *90*, 044301, doi:10.1103/PhysRevLett.90.044301.

Denlinger, R. P. (1987), A model for generation of ash clouds by pyroclastic flows, with application to the 1980 eruptions at Mount St. Helens, Washington, *J. Geophys. Res.*, *92*, 10,284–10,298, doi:10.1029/JB092iB10p10284.

Doyle, E. E., H. E. Huppert, G. Lube, H. M. Mader, and R. S. J. Sparks (2007), Static and flowing regions in granular collapses down channels: Insights from a sedimenting shallow water model, *Phys. Fluids*, *19*, 106601, doi:10.1063/1.2773738.

Dressler, R. F. (1954), Comparison of theories and experiments for the hydraulic dam-break wave, *Int. Assoc. Sci. Hydrol. Publ.*, *3*(38), 319–328.

Druitt, T. H., (1998), Pyroclastic density currents, in *The Physics of Explosive Volcanic Eruptions*, edited by J. S. Gilbert and R. S. J. Sparks, *Geol. Soc. Spec. Publ.*, *145*, 145–182.

Druitt, T. H., E. S. Calder, P. D. Cole, R. P. Hoblitt, S. C. Loughlin, G. E. Norton, L. J. Ritchie, R. S. J. Sparks, and B. Voight (2002), Small volume, highly mobile pyroclastic flows formed by rapid sedimentation from pyroclastic surges at Soufrière Hills Volcano, Montserrat: An important volcanic hazard, in *The Eruption of Soufrière Hills Volcano, Montserrat, From 1995 to 1999*, *Mem. Geol. Soc. London*, vol. 21, edited by T. H. Druitt and B. P. Kokelaar, pp. 263–279, Geol. Soc. of London, London.

Druitt, T. H., G. Avard, G. Bruni, P. Lettieri, and F. Maez (2007), Gas retention in fine-grained pyroclastic flow materials at high temperatures, *Bull. Volcanol.*, *69*, 881–901, doi:10.1007/s00445-007-0116-7.

Eames, I., and M. A. Gilbertson (2000), Aerated granular flow over a horizontal rigid surface, *J. Fluid Mech.*, *424*, 169–195, doi:10.1017/S0022112000001920.

Fan, L. S., and C. Zhu (1998), *Principles of Gas-Solid Flows*, 557 pp., Cambridge Univ. Press, Cambridge, U. K.

Fisher, R. V. (1966), Mechanism of deposition from pyroclastic flow, *Am. J. Sci.*, *264*, 350–363.

Fisher, R. V. (1995), Decoupling of pyroclastic currents: Hazards assessments, *J. Volcanol. Geotherm. Res.*, *66*, 257–263, doi:10.1016/0377-0273(94)00075-R.

Forterre, Y., and O. Pouliquen (2008), Flows of dense granular media, *Annu. Rev. Fluid Mech.*, *40*, 1–24, doi:10.1146/annurev.fluid.40.111406.102142.

Freundt, A., and M. Bursik (1998), Pyroclastic flow transport mechanisms, in *From Magma to Tephra: Modelling Physical Processes of Explosive Volcanic Eruptions*, edited by A. Freundt and M. Rosi, pp. 173–245, Elsevier, Amsterdam.

GDR MiDi (2004), On dense granular flows, *Eur. Phys. J. E*, *14*, 341–365.

Geldart, D. (1973), Types of gas fluidization, *Powder Technol.*, *7*, 285–292, doi:10.1016/0032-5910(73)80037-3.

Girolami, L., T. H. Druitt, O. Roche, and Z. Khrabrykh (2008), Propagation and hindered settling of laboratory ash flows, *J. Geophys. Res.*, *113*, B02202, doi:10.1029/2007JB005074.

Graf, W. H., and M. S. Altinakar (2000), *Hydraulique Fluviale*, 627 pp., Presses Polytech. et Univ. Romandes, Lausanne, Switz.

Hogg, A. J., and D. Pritchard (2004), The effects of hydraulic resistance on dam-break and other shallow inertial flows, *J. Fluid Mech.*, *501*, 179–212, doi:10.1017/S0022112003007468.

Hogg, A. J., and A. W. Woods (2001), The transition from inertia- to bottom-drag-dominated motion of turbulent gravity currents, *J. Fluid Mech.*, *449*, 201–224, doi:10.1017/S0022112001006292.

Hunt, M. L., R. Zenit, C. S. Campbell, and C. E. Brennen (2002), Revisiting the 1954 suspension experiments of R. A. Bagnold, *J. Fluid Mech.*, *452*, 1–24, doi:10.1017/S0022112001006577.

Huppert, H. E. (2006), Gravity currents: A personal perspective, *J. Fluid Mech.*, *554*, 299–322, doi:10.1017/S002211200600930X.

Ishida, M., H. Hatano, and T. Shirai (1980), The flow of solid particles in an aerated inclined channel, *Powder Technol.*, *27*, 7–12, doi:10.1016/0032-5910(80)85035-2.

Iverson, R. M. (1997), The physics of debris flows, *Rev. Geophys.*, *35*, 245–296, doi:10.1029/97RG00426.

Iverson, R. M., and R. G. LaHusen (1989), Dynamic pore-pressure fluctuations in rapidly shearing granular materials, *Science*, *246*, 796–799, doi:10.1126/science.246.4931.796.

Jánosi, I. M., D. Jan, K. G. Szabó, and T. Tél (2004), Turbulent drag reduction in dam-break flows, *Exp. Fluids*, *37*, 219–229.

Johnson, P. C., and R. Jackson (1987), Frictional-collisional constitutive relations for granular materials, with application to plane shearing, *J. Fluid Mech.*, *176*, 67–93, doi:10.1017/S0022112087000570.

Johnson, P. C., P. Nott, and R. Jackson (1990), Frictional-collisional equations of motion for particulate flows and their application to chutes, *J. Fluid Mech.*, *210*, 501–535, doi:10.1017/S0022112090001380.

Jop, P., Y. Forterre, and O. Pouliquen (2006), A constitutive law for dense granular flows, *Nature*, *441*, 727–730, doi:10.1038/nature04801.

Kelfoun, K., P. Palacio, D. Barba, and P. Samaniego (2008), Pyroclastic flow simulation and frictional behavior: Confrontation with a well constrained eruption at Tungurahua Volcano (Ecuador), *Bull. Volcanol.*, in press.

Kerswell, R. R. (2005), Dam break with Coulomb friction: A model for granular slumping?, *Phys. Fluids*, *17*, 057101, doi:10.1063/1.1870592.

Lajeunesse, E., J. B. Monnier, and G. M. Homsy (2005), Granular slumping on a horizontal surface, *Phys. Fluids*, *17*, 103302, doi:10.1063/1.2087687.

Larrieu, E., L. Staron, and E. J. Hinch (2006), Raining into shallow water as a description of the collapse of a column of grains, *J. Fluid Mech.*, *554*, 259–270, doi:10.1017/S0022112005007974.

Lauber, G., and W. H. Hager (1998), Experiments to dam break wave: Horizontal channel, *J. Hydraul. Res.*, *36*, 291–307.

Leal, J. G. A. B., R. M. L. Ferreira, and A. H. Cardoso (2006), Dam-break wave-front celerity, *J. Hydraul. Eng.*, *132*, 69–76, doi:10.1061/(ASCE)0733-9429(2006)132:1(69).

Levine, A. H., and S. W. Kieffer (1991), Hydraulics of the August 7, 1980, pyroclastic flow at Mount St. Helens, Washington, *Geology*, *19*, 1121–1124, doi:10.1130/0091-7613(1991)019<1121:HOTAPF>2.3.CO;2.

Lube, G., H. E. Huppert, R. S. J. Sparks, and M. A. Hallworth (2004), Axisymmetric collapses of granular columns, *J. Fluid Mech.*, *508*, 175–199, doi:10.1017/S0022112004009036.

Lube, G., H. E. Huppert, R. S. J. Sparks, and A. Freundt (2005), Collapses of two-dimensional granular columns, *Phys. Rev. E*, *72*, 041301, doi:10.1103/PhysRevE.72.041301.

Mangeney, A., F. Bouchut, N. Thomas, J.-P. Vilotte, and M. O. Bristeau (2007), Numerical modeling of self-channeling granular flows and of their levee-channel deposits, *J. Geophys. Res.*, *112*, F02017, doi:10.1029/2006JF000469.

McEwen, A. S., and M. C. Malin (1989), Dynamics of Mount St. Helens' 1980 pyroclastic flows, rockslide-avalanche, lahars, and blast, *J. Volcanol. Geotherm. Res.*, *37*, 205–231, doi:10.1016/0377-0273(89)90080-2.

Montserrat, S., A. Tamburrino, Y. Niño, and O. Roche (2007), Kinematics and pore pressure dynamics in aerated granular flows, paper presented at 32nd Congress of IAHR, Venice, Italy.

Naef, D., D. Rickenmann, P. Rutschmann, and B. W. McArdell (2006), Comparison of flow resistance relations for debris flows using a one-dimensional finite element simulation model, *Nat. Hazards Earth Syst. Sci.*, *6*, 155–165.

Neri, A., T. Esposti Ongaro, G. Menconi, M. De'Michieli Vitturi, C. Cavazzoni, G. Erbacci, and P. J. Baxter (2007), 4D simulation of explosive eruption dynamics at Vesuvius, *Geophys. Res. Lett.*, *34*, L04309, doi:10.1029/2006GL028597.

Pouliquen, O. (1999), Scaling laws in granular flows down rough inclined planes, *Phys. Fluids*, *11*, 542–548, doi:10.1063/1.869928.

Rhodes, M. J. (1998), *Introduction to Particle Technology*, John Wiley, Chichester, U. K.

Ritter, A. (1892), Die fortpflanzung der wasserwellen, *Z. Ver. Dtsch. Ing.*, *36*, 947–954.

Roche, O., M. Gilbertson, J. C. Phillips, and R. S. J. Sparks (2002), Experiments on deaerating granular flows and implications for pyroclastic flow mobility, *Geophys. Res. Lett.*, *29*(16), 1792, doi:10.1029/2002GL014819.

Roche, O., M. A. Gilbertson, J. C. Phillips, and R. S. J. Sparks (2004), Experimental study of gas-fluidized granular flows with implications for pyroclastic flow emplacement, *J. Geophys. Res.*, *109*, B10201, doi:10.1029/2003JB002916.

Roche, O., M. Gilbertson, J. C. Phillips, and R. S. J. Sparks (2005), Inviscid behavior of fines-rich pyroclastic flows inferred from experiments on gas-particle mixtures, *Earth Planet. Sci. Lett.*, *240*, 401–414, doi:10.1016/j.epsl.2005.09.053.

Saucedo, R., J. L. Macias, M. F. Sheridan, M. I. Bursik, and J. C. Komorowski (2005), Modeling of pyroclastic flows of Colima Volcano, Mexico: Implications for hazard assessment, *J. Volcanol. Geotherm. Res.*, *139*, 103–115, doi:10.1016/j.jvolgeores.2004.06.019.

Savage, S. B. (1984), The mechanics of rapid granular flows, *Adv. Appl. Mech.*, *24*, 289–366.

Savage, S. B., and K. Hutter (1989), The motion of a finite mass of granular material down a rough incline, *J. Fluid Mech.*, *199*, 177–215, doi:10.1017/S0022112089000340.

Sheridan, M. F., A. J. Stinton, A. Patra, E. B. Pitman, A. Bauer, and C. C. Nichita (2005), Evaluating Titan2D mass-flow model using the 1963 Little Tahoma peak avalanches, Mount Rainier, Washington, *J. Volcanol. Geotherm. Res.*, *139*, 89–102, doi:10.1016/j.jvolgeores.2004.06.011.

Sparks, R. S. J. (1976), Grain size variations in ignimbrites and implications for the transport of pyroclastic flows, *Sedimentology*, *23*, 147–188, doi:10.1111/j.1365-3091.1976.tb00045.x.

Sparks, R. S. J. (1978), Gas release rates from pyroclastic flows: A assessment of the role of fluidisation in their emplacement, *Bull. Volcanol.*, *41*, 1–9, doi:10.1007/BF02597679.

Sparks, R. S. J., and L. Wilson (1976), A model for the formation of ignimbrite by gravitational column collapse, *J. Geol. Soc. London*, *132*, 441–451, doi:10.1144/gsjgs.132.4.0441.

Takahashi, T., and H. Tsujimoto (2000), A mechanical model for Merapi-type pyroclastic flow, *J. Volcanol. Geotherm. Res.*, *98*, 91–115, doi:10.1016/S0377-0273(99)00193-6.

Valentine, G. A., and K. H. Wohletz (1989), Environmental hazards of pyroclastic flows determined by numerical models, *Geology*, *17*, 641–644, doi:10.1130/0091-7613(1989)017<0641:EHOPFD>2.3.CO;2.

Wadge, G., P. Jackson, S. M. Bower, A. W. Woods, and E. Calder (1998), Computer simulations of pyroclastic flows from dome collapse, *Geophys. Res. Lett.*, *25*(19), 3677–3680, doi:10.1029/98GL00710.

White, F. M. (2003), *Fluid Mechanics*, 5th ed., 866 pp., McGraw-Hill, Boston, Mass.

Whitham, G. B. (1955), The effects of hydraulic resistance in the dam-break problem, *Proc. R. Soc. London, Ser. A*, *227*, 399–407, doi:10.1098/rspa.1955.0019.

Wilson, C. J. N. (1980), The role of fluidization in the emplacement of pyroclastic flows: An experimental approach, *J. Volcanol. Geotherm. Res.*, *8*, 231–249, doi:10.1016/0377-0273(80)90106-7.

Wilson, C. J. N. (1984), The role of fluidization in the emplacement of pyroclastic flows, 2: Experimental results and their interpretation, *J. Volcanol. Geotherm. Res.*, *20*, 55–84, doi:10.1016/0377-0273(84)90066-0.

Wilson, C. J. N. (1986), Pyroclastic flows and ignimbrites, *Sci. Prog.*, *70*, 171–207.

Zenit, R. (2005), Computer simulations of the collapse of a granular column, *Phys. Fluids*, *17*, 031703, doi:10.1063/1.1862240.

S. Montserrat, Y. Niño, and A. Tamburrino, Department of Civil Engineering, Universidad de Chile, Casilla 228-3, Santiago, Chile.

O. Roche, Laboratoire Magmas et Volcans, OPGC, Université Blaise Pascal, IRD, CNRS, 5 Rue Kessler, F-63038 Clermont-Ferrand, France. (o.roche@opgc.univ-bpclermont.fr)